J. Fluid Mech. (1996), *vol.* 315, *pp.* 151–173

Nonlinear behaviour of contained inertia waves

By RICHARD MANASSEH†

Department of Applied Mathematics and Theoretical Physics, University of Cambridge, Silver Street, Cambridge CB3 9EW, UK

(Received 19 December 1994 and in revised form 26 October 1995)

Rotating fluid-filled containers are systems which admit inertial oscillations, which at appropriate frequencies can be represented as inertia wave modes. When forced by a time-dependent perturbation, systems of contained inertia waves have been shown, in a number of experimental studies, to exhibit complex and varied breakdown phenomena. It is particularly hard to determine a forcing amplitude below which breakdowns do not occur but at which linear wave behaviour is still measurable. In this paper, experiments are presented where modes of higher order than the fundamental are forced. These modes exhibit more complex departures from linear inviscid behaviour than the fundamental mode. However, the experiments on higher-order modes show that instabilities begin at nodal planes. It is shown that even a weakly nonlinear contained inertia-wave system is one in which unexpectedly efficient interactions with higher-order modes can occur, leading to ubiquitous breakdowns. An experiment with the fundamental mode illustrates the system's preference for complex transitions to chaos.

1. Introduction

1.1. *The nature of contained inertia waves*

There has been a long but sporadic history of investigations into contained rotating fluids. These are systems which admit wave motion, owing to the action of the Coriolis force as a 'restoring force'. The waves are usually called inertia waves or sometimes inertia-Coriolis waves. They are found in many contexts, including the oceans and atmosphere. However, in a contained rotating-fluid system, there are no free surfaces and the fluid is completely enclosed in a container. Complex phenomena can result from this imposition of boundary conditions. Contained inertia waves occur in the Earth's fluid outer core (Aldridge & Lumb 1987), in the fuel tanks of spinning spacecraft (Manasseh 1993) and inside some military projectiles. The mathematical problem for inertial oscillations was first formulated by Poincaré (1910), although a solution particular to cylindrical boundary conditions was found by Kelvin (1880).

Consider first the linear theory. The form of three-dimensional wave equation appropriate to a rotating fluid becomes an ill-posed problem when coupled with the boundary conditions under consideration here. Once an oscillatory time dependence has been specified, the problem comprises a hyperbolic partial differential equation, with boundary conditions normally associated with elliptic partial differential equations. Formally, theorems demonstrating the existence and uniqueness of solutions cannot be found for such a system. The possible absence of any solution (a wave

† Current affiliation: CSIRO DBCE, PO Box 56, Highett, VIC 3190, Melbourne, Australia.

mode satisfying the boundary conditions) raises the possibility of unsteady or disorganized behaviour. The lack of uniqueness is manifested in an eigenvalue problem with an infinity of solutions. If a solution happens to be found, it will be one of a spectrum of eigenmodes. The solutions that have been found so far have been for quite simple geometries, like cylinders and spheroids. In certain geometries, like a cone spinning about its axis, no modal solution may be possible. Experiments on a cone by Beardsley (1970) and numerical studies by Henderson & Aldridge (1992) supported this prediction. Where a modal structure cannot be theoretically found, both physical and numerical experiments show only small-scale disorder.

Experimental investigations where inertia waves were forced began with Fultz (1959), who investigated axisymmetric oscillations in a cylinder. Studies into a precessing cylinder (Johnson 1967) and spheroid (Malkus 1968) followed. Further experiments in cylindrical geometries (McEwan 1970; Stergiopoulos & Aldridge 1982; Manasseh 1992; 1994; Kobine 1995) confirmed the presence of inertia wave modes for this geometry, while raising doubts about their stability.

1.2. *Breakdown of contained inertia waves*

Ordered wave-modal behaviour, even in cylinders and spheroids, seems to be highly susceptible to flow instabilities and breakdown. Johnson (1967) precessed a right circular cylindrical tank and forced the system at the first mode resonance. He noted a "very turbulent-looking flow pattern". Malkus (1968) precessed a spheroid through an angle of 30° and reported violent disorder beyond a certain precession frequency. Instabilities on shear layers along characteristics were originally suspected to be the cause of the turbulence reported by Malkus. Today, elliptical-flow instabilities are thought to be the cause. Recent work on elliptical flows will be summarized shortly.

McEwan (1970), Gans (1984), Whiting (1981) and Stergiopoulos & Aldridge (1982) all reported instabilities and turbulence in similar experiments. McEwan (1970) used the term *resonant collapse* to describe breakdowns he observed.

Manasseh (1992, referred to herein as M92) catalogued the various breakdown phenomena in a cylinder and concluded that there were a variety of different processes at work. The breakdown phenomena ranged from 'violent-collapses' where fine-scale turbulence was generated, to more subtle intermittent breakdowns, where there were several transitions to chaos then back to order. These apparently involved interactions of the mode nearest resonance with a higher-order mode. Forcing amplitudes below which the nonlinear behaviour was not observed were often so small that hardly any response, linear or otherwise, could be detected. In Manasseh (1994, referred to herein as M94) one type of breakdown (Type B) was studied in detail, concentrating on the initial stages of the process. (The Type B breakdown occurs for weak forcing near the fundamental or (1,1,1) mode, and leads to disorder but not fine-scale turbulence.) Irreversible distortions away from the predictions of linear theory took place within a few revolutions of the commencement of forcing. M94 used an electrolytic dyeline technique that gave information on the velocities in the flow, which M92 could not do.

The theory of elliptical-flow instabilities (Gledzer, Dolzhanskii & Obukhov 1989; Malkus 1989; Waleffe 1990; Malkus & Waleffe 1991; Gledzer & Ponomarev 1992; Kerswell 1993) has received recent attention. It was suggested by Malkus & Waleffe (1991) that the breakdown of the inertia-wave mode that is created by the elliptical-flow instability is an "ubiquitous source of turbulence which by-passes lesser chaotic phases". The elliptical-flow studies have looked at instabilities of an elliptical flow that is a basic solution for the flow in certain geometries. In a cylinder with a circular cross-section, as noted by Kerswell (1993), the absence of an equivalent basic solution

precludes a similar treatment. In a spheriod, the basic state could permit an interaction between inertia wave modes whose azimuthal wavenumbers and frequencies differ by 1. This would permit an instability to be stationary in the forcing frame of reference, as observed in M92 and M94. In a cylinder, the frequencies will never exactly add up, as detailed in §4. Nevertheless, there are a number of ways in which elliptical-flow instabilities may be relevant to all inertia-wave breakdown phenomena. One of these is an interaction with an elliptical mean circulation, and is discussed in §6.

1.3. *Mean flow effects and nonlinear interactions*

A number of studies have looked at the azimuthal mean circulation which can arise in a contained inertia-wave system. Here azimuthal mean circulations are geostrophic flows, where the velocity field does not vary in the direction parallel to the rotation axis. Circular, elliptical, or other streamline patterns are possible.

On the basis of formal asymptotic theory (Thompson 1970), a small azimuthal mean circulation should be expected. Such a circulation was too small to be detected (M94) at early times in the experiment when small-amplitude approximations have some success in predicting the behaviour. Moreover, Thompson's (1970) circulation is a second-order effect, driven by the first-order inertial oscillations. Hence any influence this circulation has on inertia wave modes is at third-order level. However, experimental results suggest a more significant circulation, at later stages in the behaviour, or when violent collapses occur.

From experiments, Fultz (1959), Malkus (1968), McEwan (1970), Aldridge (1988, private communication) and Kobine (1995) all reported a significant azimuthal mean circulation. When an azimuthal mean circulation becomes established, it will 'Doppler-shift' the excitation frequency by changing the effective basic spin rate. This could provide a mechanism where an off-resonant excitation is frequency-shifted to a resonant state, then away again, in a 'tuning-detuning' process (Gunn & Aldridge 1990). Some evidence for this process is the intermittent chaos reported by McEwan (1970), Scott (1975) and M92.

Kobine (1995) measured a mean circulation using laser-Doppler velocimetry in the same system as M92 and M94. His work included a study of the (1,1,1) inertia wave mode near resonance. He showed that a breakdown occurs at approximately the same time as saturation of the oscillation amplitude and mean circulation. No experiments to date have identified the azimuthal structure of a mean circulation. Thus it could be circular, elliptical, or more complex in form. The relevance of a mean flow, in the context of elliptical-flow instabilities, is discussed in §6. However, mean flows are not directly investigated in the present paper.

The first aim of the experiments reported in this paper was to study the behaviour when modes are forced that have higher orders than the (1,1,1) mode studied in M94. It was of interest to see if similar departures from linear behaviour occur when higher-order modes are forced. The electrolytic dyeline technique of M94 had not been applied to modes other than the (1,1,1) mode.

As an aside in a paper on waves in a stratified fluid, McEwan (1971) speculated that the resonant collapse of inertia wave modes was caused by nonlinear interactions of triads of waves. Here he invoked the analogy between stratified and rotating flows. The degeneration of internal waves in a stratified fluid was successfully modelled by a triad mechanism (McEwan, Mander & Smith 1972; McEwan 1983). Aldridge & Stergiopoulos (1991) inferred that mode amplitudes in a cylinder were slowly oscillating with time, owing to nonlinear interactions. In M92 image-processing measurements gave some evidence of mode interactions during the Type B breakdown. In addi-

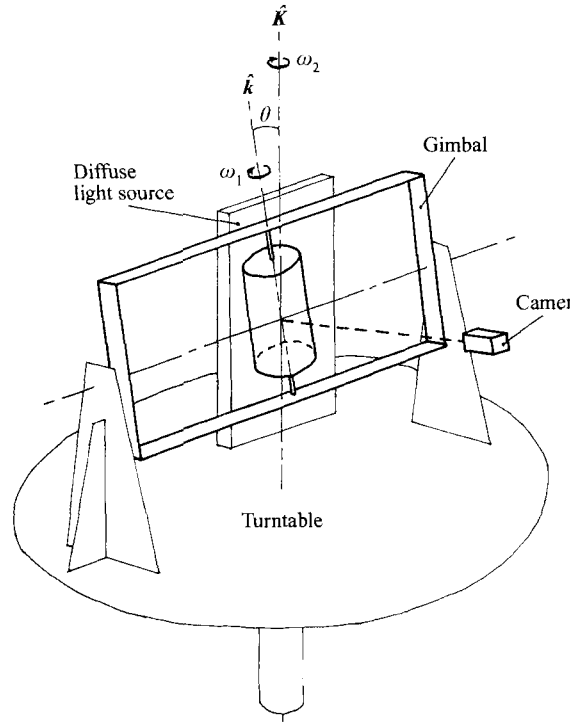

FIGURE 1. Schematic drawing of the apparatus.

tion, in observations of Type C, F and G breakdowns (M92), it appeared as though one or two secondary modes were interacting with the primary mode – the forced mode nearest resonance. Thus, McEwan's (1971) speculation on triad interactions in a cylinder should be investigated.

Section 2 is an overview of the linear theory for the system. Section 3 presents experiments indicating that departures from linear inviscid behaviour occur in more complex ways for higher-order modes. Section 4 outlines features of the weakly nonlinear theory and §5 describes an experiment showing that the fundamental-mode breakdown is not consistent with one of the simplest triad interaction models. Finally, §6 summarizes ideas on the cause or causes of the phenomena.

2. Formulation

Refer to figure 1 for some definitions of parameters. The formulation leading to a description of inertia wave modes in a fluid-filled cylinder has already been detailed (Manasseh 1991; M94), where full definitions of the terms can also be found. Here, too, the cylinder spinning about the $\hat{\boldsymbol{k}}$-axis is subjected to a forced precession or coning motion about the $\hat{\boldsymbol{K}}$-axis. The $\hat{\boldsymbol{k}}$-axis is fixed in the cylinder while the $\hat{\boldsymbol{K}}$-axis is fixed in inertial space. Rotation rates are sufficient to render the Ekman number E representing viscous effects small, $O(10^{-5})$. The incompressible, inviscid and fully nonlinear momentum equation relative to axes fixed in the container is

$$\frac{\partial \boldsymbol{u}}{\partial t} + (\boldsymbol{u}\cdot\nabla)\boldsymbol{u} + 2\hat{\boldsymbol{k}}\times\boldsymbol{u} + 2(\omega_2/\omega_1)\hat{\boldsymbol{K}}\times\boldsymbol{u} + (\omega_2/\omega_1)(\hat{\boldsymbol{K}}\times\hat{\boldsymbol{k}})\times\boldsymbol{r} + [(\hat{\boldsymbol{k}}+(\omega_2/\omega_1)\hat{\boldsymbol{K}})\times\omega_1((\hat{\boldsymbol{k}}+(\omega_2/\omega_1)\hat{\boldsymbol{K}})\times\boldsymbol{r})] = -\nabla P, \tag{2.1}$$

where $\mathbf{r}$ is the location of a fluid element within the container, $\boldsymbol{u}$ is the fluid velocity and P is pressure. In subsequent analyses a *reduced pressure* p is used, which incorporates the steady components of the centrifugal term. Note that $\hat{\boldsymbol{K}}$ varies with time. The linearized form of (2.1) is obtained by treating the *nutation angle* θ between $\hat{\boldsymbol{k}}$ and $\hat{\boldsymbol{K}}$ as small and formally expanding $\boldsymbol{u}$ and p in powers of θ. This gives to leading order

$$\frac{\partial \boldsymbol{u}}{\partial t} + \omega \hat{\boldsymbol{k}} \times \boldsymbol{u} + \nabla p = -(\omega - 2)(r \cos(\phi + t))\hat{\boldsymbol{k}}, \tag{2.2}$$

where $\omega = 2(1 + \omega_2/\omega_1)$. The incompressibility condition is given by

$$\nabla \cdot \boldsymbol{u} = 0\,. \tag{2.3}$$

The boundary condition is

$$\boldsymbol{u} \cdot \hat{\boldsymbol{n}} = 0\,, \tag{2.4}$$

where $\hat{\boldsymbol{n}}$ is the unit normal vector to the container surface. This allows a free-slip condition at the container wall consistent with the assumption of an inviscid flow. Cylindrical polar coordinates (r, ϕ, z) fixed in the container with their origin at the cylinder centroid are used. Appropriate simplifications of the governing equations, including the presumption of wave-modal behaviour, lead to Poincaré's equation,

$$\frac{1}{r}\frac{\partial}{\partial r}\left(r\frac{\partial Q_n}{\partial r}\right) + \frac{1}{r^2}\frac{\partial^2 Q_n}{\partial \phi^2} + (1 - \omega^2)\frac{\partial^2 Q_n}{\partial z^2} = 0\,, \tag{2.5}$$

in the pressure amplitude Q_n of the nth mode; (2.5) is a hyperbolic p.d.e. for $|\omega| > 1$, when the characteristic surfaces are cones with half-angle $\tan^{-1}(\omega^2 - 1)^{-1/2}$. The relevant solution is

$$Q_n = J_m(2\lambda_n r)\cos(2(\omega^2 - 1)^{-1/2}\lambda_n[z + h/2])\, \mathrm{e}^{\mathrm{i}m\phi}, \tag{2.6}$$

where J_m is the Bessel function of the first kind, order m, and h is the cylinder height/radius ratio. The modes arising from precessional forcing have azimuthal wavenumber $m = 1$ (since the forcing term on the right-hand side of (2.2) goes as $\cos(\phi + t)$). The radial wavenumbers are given by the roots of

$$\lambda \frac{\partial J_m(\lambda)}{\partial r} + m\omega J_m(\lambda) = 0, \tag{2.7}$$

in order to satisfy the radial boundary condition. In order to satisfy the axial boundary condition with integer axial wavenumber k,

$$\omega^2 = 1 + \left(\frac{\lambda_{klm} h}{k\pi}\right)^2, \tag{2.8}$$

where λ_{klm} is the lth root of (2.7). Hence the argument of the Bessel functions λ is non-integer but l is the index that counts the number of radial cycles. Resonant excitation frequencies are thus values of ω satisfying (2.7) and (2.8). Some of the lower-order ω_n are given in table 1 for the h used here, including some modes that cannot be precessionally forced.

3. Experiments with higher-order modes

Here the early-time behaviour of the system, for modes of higher order than the fundamental or (1,1,1) mode, is examined. The (1,1,1) mode rapidly and irreversibly departed from linear predictions (M94), in both the time dependence and the flow

k	l	m	ω_{klm}	λ_{klm}	k	l	m	ω_{klm}	λ_{klm}	k	l	m	ω_{klm}	λ_{klm}
1	1	0	−3.403	3.832	1	1	1	−4.056	4.631	1	1	2	−4.893	5.642
1	2	0	−6.038	7.016	1	2	1	−6.733	7.844	1	2	2	−7.649	8.934
2	1	0	−1.909	7.016	2	1	1	−2.305	4.893	2	1	2	−2.712	5.939
2	2	0	−3.141	1.017	2	2	1	−3.590	8.124	2	2	2	−4.050	9.246
3	1	0	−1.475	3.832	3	1	1	−1.732	4.996	3	1	2	−1.994	6.098
3	2	0	−2.223	7.016	3	2	1	−2.537	8.239	3	2	2	−2.846	9.419
1	1	0	3.403	3.832	1	1	1	2.643	2.882	1	1	2	4.014	4.580
1	2	0	6.038	7.016	1	2	1	5.278	6.105	1	2	2	6.755	7.870
2	1	0	1.909	3.832	2	1	1	1.484	2.584	2	1	2	2.056	4.234
2	2	0	3.141	7.016	2	2	1	2.654	5.792	2	2	2	3.346	7.523
3	1	0	1.475	3.832	3	1	1	1.224	2.493	3	1	2	1.524	4.063
3	2	0	2.223	7.016	3	2	1	1.891	5.674	3	2	2	2.304	7.336

TABLE 1. Resonant excitation frequencies ω_{klm} and radial wavenumbers λ_{klm} for a cylinder, $h = 8/3$

structure. The time dependence lost its oscillatory nature. The flow structure developed a 'kink' at the container centroid, representing a flow with about 1/5 of the linear response magnitude. The (3,1,1) and (5,2,1) modes were selected for this study because they are the most readily forced with the experimental equipment, after the (1,1,1) mode.

Figure 1 illustrates the apparatus. The equipment, experimental procedure and electrolytic dyeline flow-visualization method are as detailed in M94; here is a brief summary. The system is spun up to solid-body rotation with the axes of spin and precession collinear ($\theta = 0$). However, the rotation frequencies of the container (ω_1) and turntable (ω_2) are set at a combination that would excite the desired mode if θ were non-zero. At time $t = 0$, the spin axis is tilted to smoothly increase θ to 1°. This begins forcing of the system. The descriptions below are summaries of observations of several identical runs, which show both qualitative and quantitative repeatability. Owing to the nature of the dyeline technique, observations are possible for a few tens of revolutions before the dyeline disspates. For consistency with M92 and M94, the non-dimensional times quoted here are scaled by ω_1, which was 10.47 rad s^{-1} (1.67 Hz). Hence times are in revolutions of the container relative to the turntable and camera shown in figure 1.

3.1. *Experiments in the (3,1,1)-mode range*

Here the behaviour for $1.22 \leqslant \omega \leqslant 1.28$ for a nutation angle of $\theta = 1°$ was studied. From M92, forms of breakdown classified as Type F and F1 collapses (and Type E, at $\omega = 1.28$) are to be expected in this frequency range. These breakdowns result in weak turbulence (with scales of about 1/4 of the container diameter). They can be followed by intermittent chaos – a quasi-periodic re-ordering of the flow and subsequent recurring breakdowns. A nutation angle of 1° was used because it was anticipated from M94 that stronger forcing would result in inadequate dyeline formation.

Experiments were run at $\omega = 1.22, 1.24, 1.26$ and 1.28. The theoretical value of ω at the (3,1,1)-mode resonance is 1.2237. From M92, in which a different visualization technique was used, the breakdowns at these parameter values are expected to occur over timescales of 50 to 100 revolutions. By this time the dyelines would have virtually disappeared. There were five runs at each ω. In the following descriptions, the term *nodal* planes refers to planes of constant z where the radial and azimuthal velocities

(*a*) (*b*)

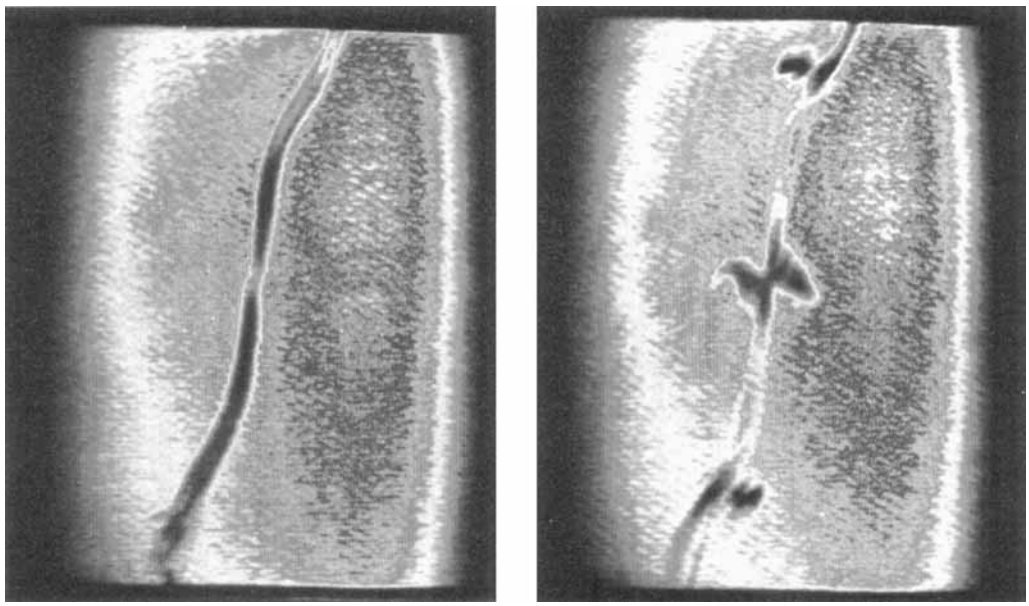

FIGURE 2. (*a*) Dyeline pattern for $\omega = 1.28$, $\theta = 1°$. The time is 3.6 ± 0.3 non-dimensionally. The image is taken from the videotape record at 2.19 s. The timing error arises from a 0.2 s uncertainty in the time of commencement of forcing. The image was enhanced using standard histogram-equalization and intensity-mapping techniques; variations in the background are caused by noise at intensity levels unrelated to the dyeline image. (*b*) As (*a*) but for $\omega = 1.22$. The time is 3.5 ± 0.3 non-dimensionally or 2.18 s on the videotape record.

are zero and the axial velocity is an extremal. *Antinodal* planes are planes where the radial and azimuthal velocities are extremal and the axial velocity is zero.

Note that the flange of the tank which appears at the top of the image in figure 2 obscures the top 1/12 of the image of the fluid interior. This gives a false impression of the position of the tank top plane relative to the centre.

Figure 2(*a*) shows the forced response for $\theta = 1°$ and $\omega = 1.28$ (about 5% away from the (3,1,1)-mode resonance) at 3.5 ± 0.3 revolutions after the commencement of forcing. A sinusoidal dyeline displacement with $1\frac{1}{2}$ axial wavelengths can be seen, as expected from linear inviscid theory for the (3,1,1) mode. The amplitude here is too small for reliable estimation, but it will be estimated shortly for $\omega = 1.22$. The flow for $\omega = 1.28$ is not steady at the stage of figure 2(*a*), and develops as described below for $\omega = 1.22$.

Figure 2(*b*) shows the forced response for $\theta = 1°$ and $\omega = 1.22$, which is much closer to the theoretical resonance at $\omega = 1.2237$, at 3.5 ± 0.3 revolutions after the commencement of forcing. There are outflows of dye at the central (3,1,1)-mode nodal plane. The outflows spread in a plane containing the z-axis and in a direction at approximately 50° to the z-axis. For brevity, this dye structure will be called a *bow-tie*. Outflows also occur at the upper and lower (3,1,1)-mode nodal planes, where, however, outflows are more prominent on one side of the wire than on the other. It is not clear if this is due to the wire being diagonal or if it represents an asymmetry in the behaviour. All the outflows appear to be coplanar and in a plane containing the z-axis. As with the kink in the (1,1,1)-mode dyeline (M94) the outflow pattern rotates with the container. This is in contrast to the linear forced response which

is steady in the turntable (forcing) frame of reference, apart from modulations due to the transients, 'Stokes drift' and other kinematic factors. These are comparatively small (M94).

The bow-tie pattern in figure 2(*b*) could already be discerned before $t = 0$ owing to the 'out-of-alignment forcing'. As detailed in Manasseh (1991), even very small misalignments in the apparatus, prior to the commencement of forcing, can lead to some excitation of a mode if the system is set near a resonance. At $\omega = 1.22$ this effect is particularly noticeable as the frequency is only about 0.3% away from the (3,1,1) mode resonance. Once intentional forcing commences at $\omega = 1.22$ or $\omega = 1.28$, outflows appear to generate the same patterns, overlaying those already present due to the out-of-alignment forcing. In figure 2(*b*) there has already been some smudging of the bow-tie pattern and the outflows at the upper and lower (3,1,1) mode nodal planes. Noticeable at the tip of the left wing of the bow-tie is a curvature in the dyeline path suggestive of a recirculation zone in that region of the container. This curvature is a consistent feature of all the runs for $\omega = 1.22$. Its presence on one wing of the bow-tie may be due to the fact that the wire does not pass exactly through the tank centre, rather than to any asymmetry in the behaviour.

The amplitude of what may be presumed to be the (3,1,1) mode, can be estimated from the images, as described in M94. At $\omega = 1.22$ this estimation gives a velocity amplitude of about 45 ± 10 mm s^{-1}. The scale expected for linear behaviour is about 16 mm s^{-1} (M94). The outflow producing the bow-tie corresponds to a flow of about 1 mm s^{-1}. It was not possible to say if this outflow was arrested, as did the 'kink flow' observed in the (1,1,1) mode range in M94. The dyeline at $\omega = 1.22$ had dissipated before any halt to the outflow could be discerned. There will be a further discussion in §6.

In all cases, the outflows occurred at the three nodal planes of the (3,1,1) mode.

3.2. *Experiments in the (5,2,1)-mode range*

A series of experiments was conducted to gather data spanning the frequency spectrum near the (5,2,1) mode resonance. Theoretical resonance of the (5,2,1) mode occurs when $\omega = 1.378$. Experiments were run at $\omega = 1.34, 1.36, 1.38$ and 1.40, a set of values about 10% away from the (3,1,1) mode resonance. There were five runs at each ω. However, for the first run in each set, forcing was not initiated so that the development due to the out-of-alignment of spin and precession axes could be noted. As with the (1,1,1)-mode experiments (M94) and the (3,1,1)-mode experiments described above, the nutation angle was set at $\theta = 1°$.

The behaviour at $\omega = 1.34$ when forcing was not initiated does not show the clear outflows due to the out-of-alignment forcing that were observed closer to the (3,1,1)-mode resonance. Rather, two breaks in the dyeline appear at heights of approximately $z = -h/10$ and $z = h/10$. One end of each broken portion moves radially outwards. The broken portions rotate with the tank. With this weak out-of-alignment forcing, they correspond to dye leaving the wire at a rate of about 0.13 mm s^{-1}. The broken portions are coplanar and make an angle of roughly 30° with the vertical. Similar behaviour was noted at $\omega = 1.36$, with detachments also occurring at the $z = 0$ plane. The characteristic angle of the governing equation (2.5) at $\omega = 1.34$ is 48.3°, so there is no coincidence between the angle of the detached portion and the characteristics.

The runs at $\omega = 1.34$ were the closest of the runs in the (5,2,1) mode range to the (3,1,1) resonant frequency at $\omega = 1.2237$. The behaviour after forcing commences is complicated. Initially the dyeline distorts in the pattern expected for the (3,1,1) mode,

a displacement relative to the wire that is steady in the turntable frame. By four revolutions, however, complicated developments are occurring at the central nodal plane and at planes approximately at $z = -h/3$ and $z = h/3$. These three planes are the nodal planes of the (3,1,1) mode. At the $z = \pm h/3$ planes, a portion of the dyeline of about $0.13h$ in length detaches itself from the wire. At the centre, a localized kink appears with a single wavelength in about the same length of $0.13h$. As the spatial extent of the kink grows, it becomes obvious that it is rotating with the tank.

By 10 revolutions, prominent radial outflows have developed at the central nodal plane and at $z = \pm h/3$. The outflows are roughly coplanar and all rotate with the tank. The central outflow appears like the bow-tie pattern noted above for the (3,1,1) mode. Each outflow is consistent with a flow that tears away a portion of dye at a nodal plane and carries it radially outwards. The rest of the dyeline becomes convoluted and distorted. By 30 revolutions the only dye remaining is in the torn-away portions. These have ceased their radial motion and are revolving with the tank at a radius of about $r/4$.

This behaviour, organized along the three nodal planes of a $k = 3$ mode, may be because at $\omega = 1.34$ the (3,1,1) mode could still contribute more to the flow than the (5,2,1) mode. This behaviour was also noted at $\omega = 1.36$.

After forcing commences at $\omega = 1.36$, a central radial outflow appears. This develops like the outflow at the central nodal plane at $\omega = 1.34$. The two other outflows noted at $\omega = 1.34$ also develop, again approximately at the nodal planes of a $k = 3$ mode. The development up to about 4 revolutions is the same as at $\omega = 1.34$. A $k = 3$ mode pattern appears, and this is a displacement relative to the wire that is steady in the turntable frame. After about 4 revolutions, the $2\frac{1}{2}$ axial wavelengths one would expect from the (5,2,1) mode appear. However, this new wavy displacement of the dyeline from the wire is rotating with the tank. It cannot represent the linear forced response of the (5,2,1) mode since that would be stationary in the turntable frame of reference. The initial wavy displacements of the dyeline relative to the wire in the (1,1,1)-mode and (3,1,1)-mode ranges (M94 and §3.1 above, respectively) were stationary in the turntable frame. Hence, they were consistent with the linear forced time dependences of those modes.

Figure 3(*a*) shows the situation at 6.5 revolutions. Recall that the flange at the top of the tank obscures the top 1/12 of the fluid volume, giving a false impression of the tank top plane relative to the centre. The central outflow is the most prominent, as it forms an S-shape in the vicinity of the tank centre. By about 10 revolutions, the state is as shown in figure 3(*b*). Radial outflows are not observed at any additional nodes corresponding to the (5,2,1) mode. Ultimately, the entire dyeline appears to break into several co-tangential filaments.

At $\omega = 1.38$ the (5,2,1) mode is only 0.1% away from resonance, whereas the (3,1,1) mode is now 13% away from resonance. In the first run at $\omega = 1.38$, intentional forcing was not initiated, in order to study the behaviour under the out-of-alignment forcing. Under this very weak forcing, five points where dye has collected on the wire are apparent. The five collection points appear at the nodal planes of the (5,2,1) mode. The term 'collection' is used here as it appears as if the dye has been swept towards these points by a very weak flow. This is in contrast to the clear breaks which were observed at the two lower frequencies in the (5,2,1) range. The central collection is the most prominent, with radial outflows just above and below the $z = 0$ plane. The collection nearest the tank bottom appears much fainter than the other four, which may be due a combination of effects: dirt on the wire in this region; and the asymmetry in the electric field referred to in Manasseh (1991).

(a) (b)

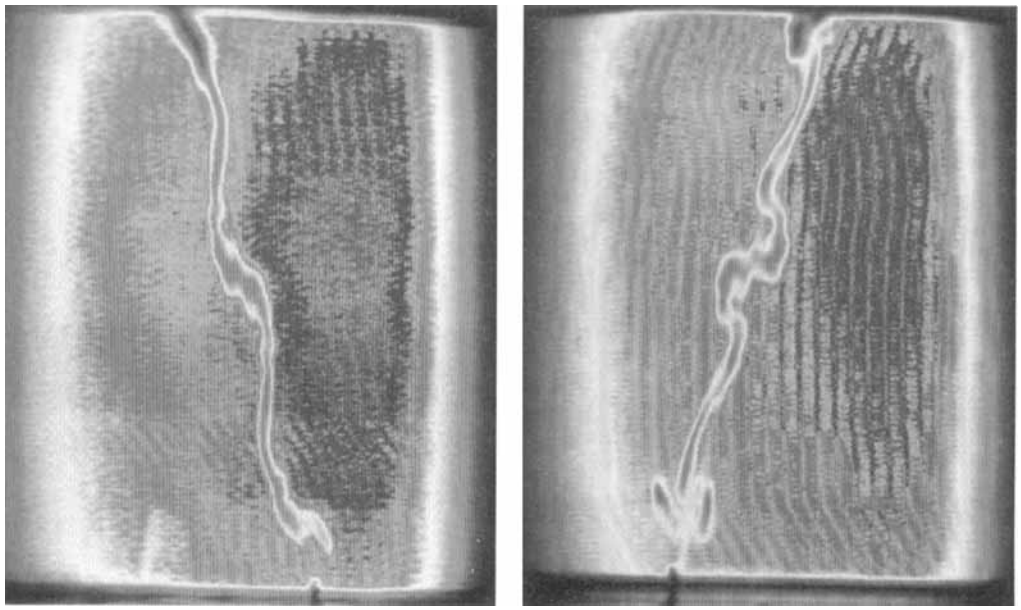

FIGURE 3. (a) Dyeline pattern for $\omega = 1.36$, $\theta = 1°$. The time is 6.5 ± 0.3 non-dimensionally or 3.90 s on the videotape record. Image enhancement as figure 2; vertical stripes in the background are due to an unavoidable enhancement of the moulded-plastic light diffusers behind the tank. (b) As (a) but time is 10.0 ± 0.3 non-dimensionally or 6.00 s on the videotape record.

Initially, after forcing commences at $\omega = 1.38$, the behaviour is similar to that at $\omega = 1.34$ and $\omega = 1.36$. The initial appearance of a $k = 3$ mode pattern can be noted: a displacement relative to the wire that is steady in the turntable frame. The radial outflows at the central nodal plane grow. Other outflows are not initially in evidence. By 4 revolutions it appears as if the dyeline is being twisted as the central outflow rotates with the tank while the $k = 3$ mode pattern continues to be stationary in the turntable frame. A revolution later, there appear $2\frac{1}{2}$ axial wavelengths, which in this $\omega = 1.38$ case do appear stationary in the turntable frame. The instantaneous appearance of this structure is virtually the same as at $\omega = 1.36$, the significant difference being the time dependence. Breaks in the dyeline at the nodal planes of a $k = 3$ mode do not appear until about 5 revolutions; the subsequent development is very similar to that at $\omega = 1.36$.

When $\omega = 1.40$ and intentional forcing was not initiated, two collections of dye on the wire are apparent, at approximately $z = -h/3$ and $z = h/3$. The second collection near the tank bottom is much weaker. After forcing commences at $\omega = 1.40$ the behaviour is similar to that at $\omega = 1.38$: there is a very prominent bow-tie outflow at the $z = 0$ plane and lesser outflows approximately at the $z = -h/3$ and $z = h/3$ planes. At this frequency, by about 10 revolutions the dyeline clearly appears to be twisted-up for $-h/3 < z < 0$ and $0 < z < h/3$. As at the other frequencies studied, the outflows at the nodal planes do not progress beyond about a quarter of the radius.

There will be some discussion of the dyeline observations in this section in §6.

4. Approximate resonant triads

In some experiments with contained inertia-wave systems there is evidence of wave interactions (Aldridge & Stergiopoulos 1991; M92 as detailed in §1). In this section a model applicable to some regions of the parameter space investigated in M92 and M94 is outlined. Here a *weak* nonlinear system is specificially defined as one which can be described by a combination of a small number (less than 10, say) of the eigenmodes described in §2, with amplitudes varying arbitrarily with time. The first aim is to illustrate the complexity of the possible nonlinear interactions for the present system. A weakly nonlinear model is most likely to apply to the 'gentler' Type B, C, F and G collapses (M92) and the early-time behaviour of M94. The second aim is to test this idea for one case; a suitable experiment will be presented in §5.

To investigate interactions between the modes, it is assumed that the flow is composed of a sum of the normal eigenmodes, each satisfying the boundary conditions and multiplied by arbitrary complex amplitudes. In investigations of the nonlinear interaction of orthogonal eigenmodes, it is often the case that the spatial structure of the modes is made up of trigonometric functions. This is the case with surface or internal ocean waves, which have been extensively studied (for example, see Thorpe 1966) or with waves in containers with rectangular boundaries (McEwan *et al.* 1972). In these cases it is possible to assume a 'resonant triad' condition $\pm\sigma_a = \pm\sigma_b \pm \sigma_c$ and $\pm\underline{k}_a = \pm\underline{k}_b \pm \underline{k}_c$, where σ is the frequency and $\underline{k}$ is the wavenumber vector, for three trigonometric modes a, b and c. Here the quadratic nonlinear terms combine two modes to force a third. The appropriate interaction equations can be inferred heuristically (Craik 1985) by equating those terms that satisfy the resonant triad condition. However, in the present case the Bessel functions which make up the spatial eigenfunctions do not obey the simple addition theorems that trigonometric functions do. Thus the wavenumbers in the radial direction need not sum to permit nonlinear interaction. Details of the required approach for a cylindrically contained inertia-wave system are in the Appendix. An *interacting set* is defined as a group of three modes whose axial and azimuthal wavenumbers sum appropriately.

Adopting an essentially standard weakly nonlinear formulation (detailed in the Appendix), it is possible to demonstrate the propensity for unexpectedly efficient interactions with higher-order modes. The root-finding algorithms used to calculate the resonant frequencies such as those presented in table 1, were expanded to produce plots indicating how close a given interacting set is to being a resonant triad.

The program works with a specified primary mode. It searches through the spectrum of secondary modes, with an algorithm that starts with low k_b and m_b and progressively increases these, finding the $\omega_b > 0$ and the $\omega_b < 0$ eigenmode with the lowest radial wavenumber for each (k_b, m_b) combination. For each such combination, there are eight potential third modes that could form an interacting set with the first two, generated by addition and subtraction of k_b, m_b and $1/\omega_b$ with k_a, m_a and $1/\omega_a$. (It is $1/\omega$ that must be used because of the way the non-dimensional frequency ω was defined; explanations are in M92.) The program determines how close the resulting potential third mode is to a true root of the transcendental equation, i.e. a solution of (2.7) and (2.8). The quotient

$$\Delta = \left| \frac{m\omega J_m(\lambda)}{\lambda J'_m(\lambda) + m\omega J_m(\lambda)} \right|,$$

which indicates the closeness to matching the resonant triad condition, is plotted in a three-dimensional histogram. Figure 4 shows the result, where the primary mode

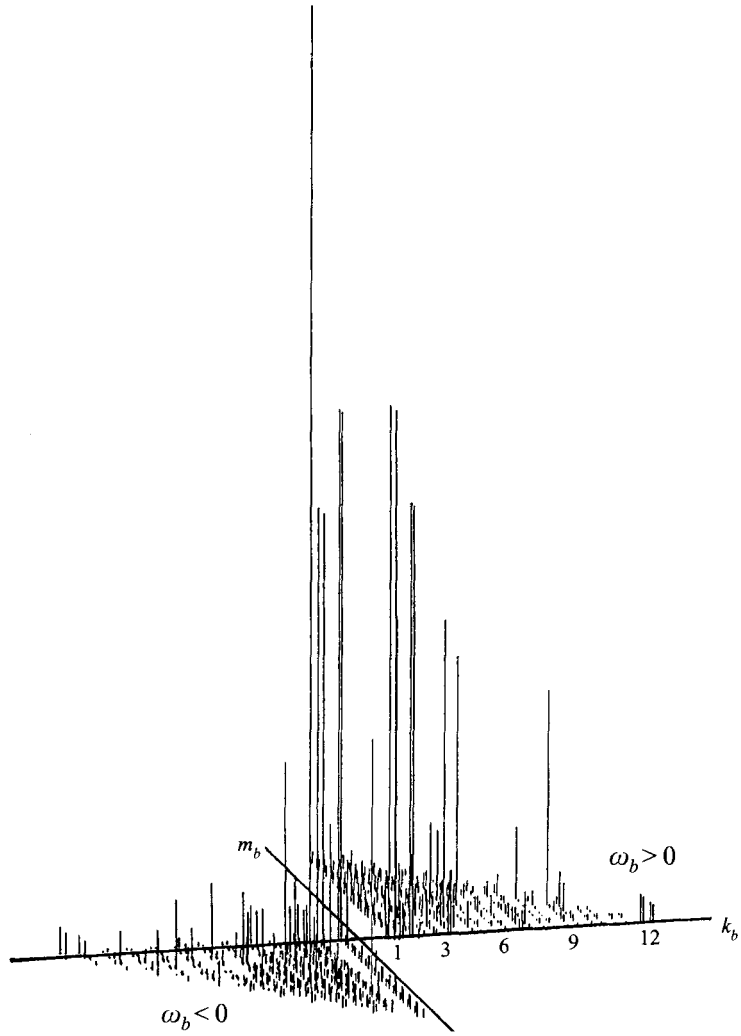

FIGURE 4. The quotient Δ that indicates the closeness to matching the resonant triad condition. The primary mode is (1,1,1); secondary modes plotted are ones with the lowest radial wavenumber, $l_b = 1$. The domain in $k_b \times m_b$ space is $-12 \leqslant k_b \leqslant 12$ and $-11 \leqslant m_b \leqslant 11$ with $m = 0$ allowed. Scales on the k_b and m_b axes are the same. The algorithm advances such that $(k_b, m_b) = (n, n - k_b)$, with $n \in \{1, 12\}$ to avoid computing modes where both k_b and m_b are high.

is the (1,1,1) mode with $\omega = 2.643$ and the horizontal plane is $k_b \times m_b$ space. The $\omega_b > 0$ secondary modes have been placed in the first quadrant and the $\omega_b < 0$ in the fourth. There are eight vertical spikes grouped around each (k_b, m_b) point in the horizontal plane, representing the eight possible Δ values. If $k_b = k_a$ half of the eight have $k_c = 0$, which cannot be an inertia wave mode. In this case, Δ is set to zero.

The process is repeated for secondary modes with higher radial wavenumbers. Figure 5 shows the result of the search up to the tenth radial wavenumber with $n_{max} = 12$. The closest interacting set to a resonant triad is the set $\{(1, 1, 1, 2.643), (3,7,1,-6.873), (2, 1, 0, 1.909)\}$ where the notation (k, l, m, ω) is being used. Here $1/\Delta$ is only 0.00061; the corresponding spike is the tallest in figure 5(f). It can be seen that the spikes are thinning out by the time $l_b = 10$ is reached. Nonetheless, there may be an important almost-resonant triad at a slightly higher radial wavenumber, or indeed

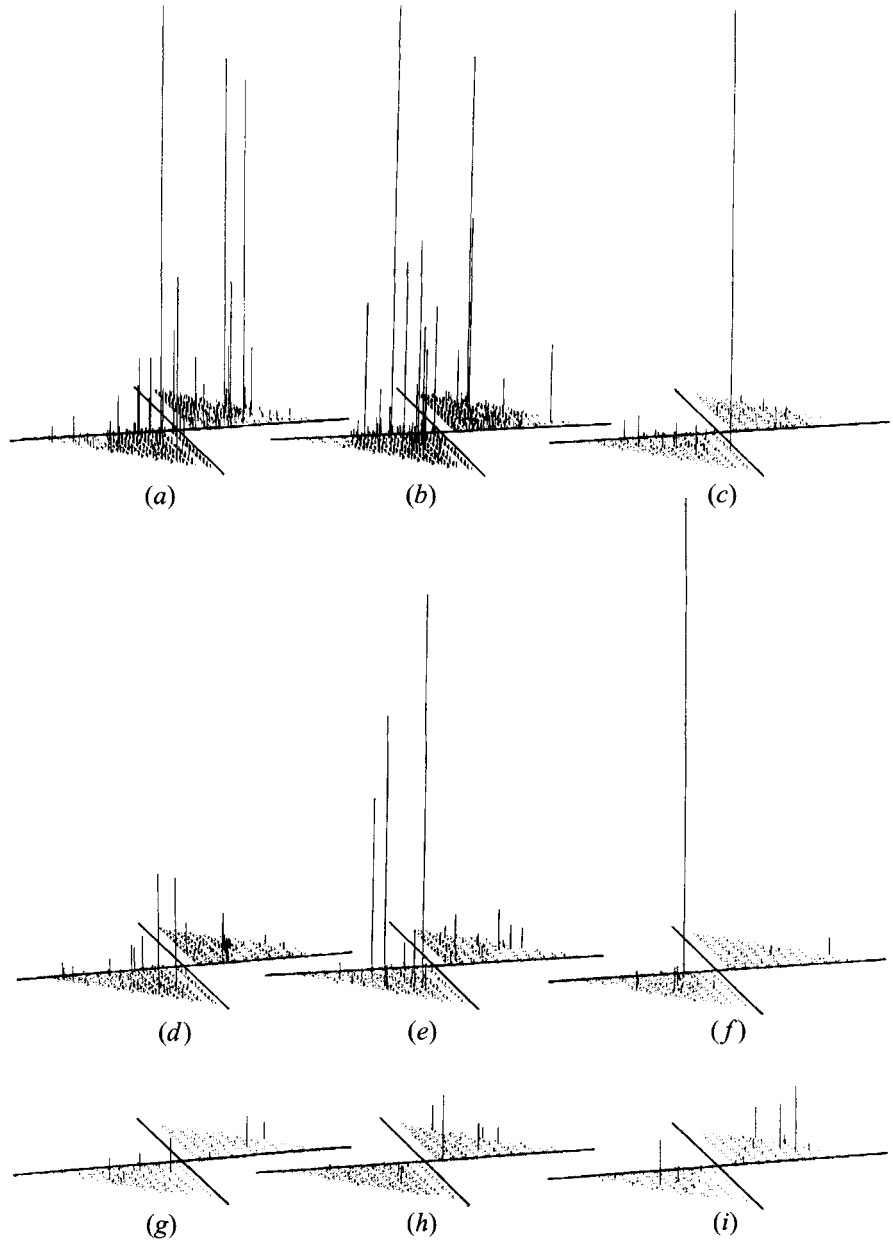

FIGURE 5. The quotient Δ for primary mode (1,1,1); secondary modes are plotted for nine higher radial wavenumbers: (*a*) $l_b = 2$ to (*i*) $l_b = 10$. The heights of all the spikes in figures 4 and 5 (*a–i*) have been normalized by the same factor.

up to radial wavenumbers of $O(E^{-1/4})$. Here, viscous damping from Stewartson layers (Greenspan 1968) would be important.

The quotient Δ is only one criterion that should be used to estimate the importance of an interacting set. The size of the nonlinear projections, the $c_{n\alpha\beta}$ defined in the Appendix, should also be used to weight the height of the spikes in figures 4 and 5. Nevertheless, it can be inferred from figure 5 that efficient interactions are likely to be both plentiful and unpredictable, owing to the transcendental nature of the dispersion

relation for these modes. An indication of the relative sizes of some $c_{n\alpha\beta}$ for a specific case will be given in §5.

5. Experiment to test a hypothesis of modal interaction

It is now of interest to test the proposition that some of the breakdown regimes may be explained by a weakly nonlinear model. The initial philosophy here will be to select interacting sets on the basis of their *simplicity*. The criteria for simplicity are the number of modes in an interacting set, and the magnitudes of their wavenumber vectors. It is suggested that the chance of a set being important in the flow is a function of its simplicity only. This selection is done without regard for the closeness of the interacting set to a resonant triad. Temporarily laying aside the indications from §4 that complex interactions are likely to be ubiquitous, we will try to use the simplest interactions to explain some experimental observations.

One of the simplest interacting sets including the (1,1,1) mode as primary is $\{(1,1,1),(2,l_2,0)\}$. An interacting set involving a mode with $m = 0$ – an axisymmetric mode – is a special case. It is a 'triad' with two members; mathematically, the third member of the triad is formed by the complex conjugate of the primary mode.

In M94 a kink was noted in the dyeline pattern and it was concluded that it represented an early failure of the linear inviscid theory. The magnitudes of flow corresponding to the kink were consistent with second-order nonlinear effects. This discrepancy between experiment and linear inviscid theory for the (1,1,1) mode may be consistent with the presence of the (2,1,0) mode as part of an interacting set $\{(1,1,1),(2,l_2,0)\}$. This is because, as described below, the kink is consistent with a flow corresponding to the (2,1,0) mode. (The closest triad identifed in §4 also involved an interaction of the (2,1,0) and (1,1,1) modes, but with a (3,7,1) mode. There was no evidence of a $k = 3$ structure that might be due to a (3,7,1) mode.)

Under weakly nonlinear theory, the flow in tank coordinates due to the (2,1,0) mode could be steady or slowly varying rather than oscillatory, because a linear time dependence is no longer being assumed. It was noted in M94 that the kink is consistent with an axisymmetric steady flow that is radially outwards at the (1,1,1)-mode nodal plane. Neither the inclusion of transients nor the inclusion as many as 13 additional higher-order linear forced modes appeared to explain the discrepancy. Viscous effects seemed unlikely. To explain the results of M94 a large radial outflow at the nodal plane and a small azimuthal component would be required. This would result from the presence of the (2,1,0) mode if its complex amplitude had an appropriate steady or slowly varying phase. Figure 6 is an illustration of how this mode could cause the kink.

The test was done by the introduction of new flow-visualization wires. (These wires generate the electrolytic dyeline that is the basis of the flow-visualization method.) Four new wires were added, equispaced around the cylinder. They were parallel to the z-axis and at half the tank radius. At this radius there is a maximum in the azimuthal and radial velocities of the (2,1,0) mode. Calibration details are in Manasseh (1991).

If the hypothesis of a simple modal interaction is correct, then on the four new wires the dyelines are predicted to deform radially. The maximum outwards deformation should be at the $z = 0$ plane and the maximum inwards deformation near the tank ends. This is illustrated in figure 6(*b*).

Experiments were run at $\omega = 2.46$ and 2.60. The nutation angle was set at $\theta = 1°$. The development of the dyeline from the central wire was as noted in M94. Initially, the dyelines on the new wires tilted in the same sense as the dyeline on the original

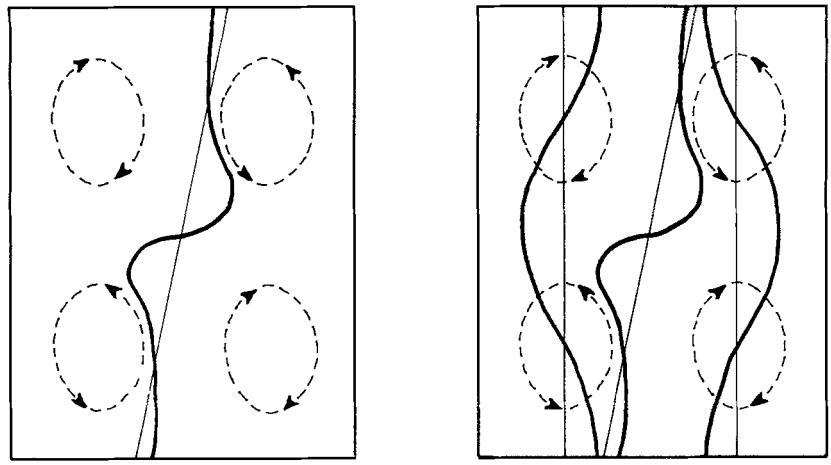

(*a*) (*b*)

FIGURE 6. Dyeline patterns created by the hypothetical presence of a (2,1,0) mode owing to a weakly nonlinear interaction with a forced (1,1,1) mode. Instantaneous streamlines due to a (2,1,0)-mode structure with appropriate slowly varying phase are shown as dashed lines. Faint straight lines are the wires generating the dye. (*a*) Pattern as described by M94. (*b*) Pattern that would be seen with additional visualization wires in the tank.

central wire. Again, this is consistent with the linear inviscid theory. This state is shown in figure 7(*a*), which is a video frame taken about 2.5 revolutions after the commencement of forcing. Here $\omega = 2.46$ and $\theta = 1°$. After a few more revolutions, new developments occur. At approximately the $z = 0$ plane, kinks appear in the dyelines on the vertical wires at the same time as the kink on the central dyeline. This is illustrated in figure 7(*b*), which is at about 5 revolutions. A small (about 1/6 of the tank height in length) patch of dye detaches from each vertical wire and moves radially slightly inwards. This motion is opposite in sense to the motion predicted by the hypothesis above. Furthermore it is much too small in scale to be accounted for by the flow due to a low-order mode like the (2,1,0) mode. In a few more revolutions, dye continues to separate from the vertical wires in the vicinity of the $z = 0$ plane. This dye forms blobs of about a fifth of the tank radius in size but never departs from the wires by more than this amount. Figure 7(*c*) is at about 7 revolutions, when the kink in the central dyeline has developed to about a third of the radius in extent. (The maximum radial development is not in the same plane as the two vertical wires in this image.) It shows that there has been hardly any radial or azimuthal motion of dye from the vertical wires mounted at half the tank radius. Rather, there is a complex collection of dye about each vertical wire, at approximately the $z = 0$ plane.

This collection of dye continues through the stage noted in M94, when the upper and lower arms of the central dyeline have wound into spiral forms. By this stage almost all the dye from the vertical wires has collected into blobs at approximately the $z = 0$ plane.

Referring to figures 7(*b*) and 7(*c*), note that the blobs on the wires at half the tank radius are not centred precisely at the $z = 0$ plane. Rather, the left-hand one is displaced slightly below this plane, and the right-hand one is slightly above it. This relative displacement appears steady in the turntable frame once the blobs have clearly formed. This displacement is consistent with the structure of the (1,1,1) mode, just as is the initial tilt of the dyeline. This affirms that the (1,1,1) mode continues

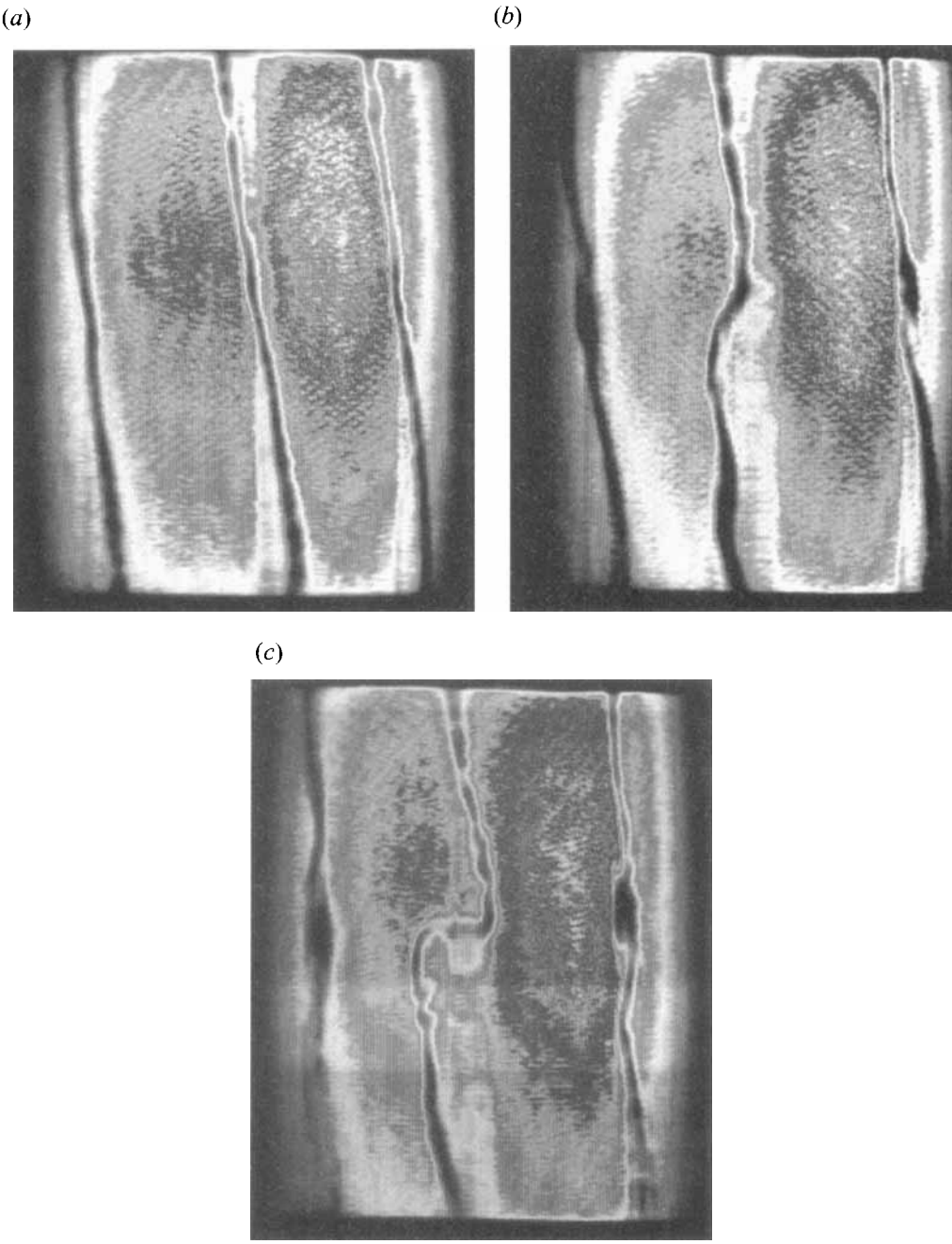

FIGURE 7. Dyeline pattern for $\omega = 2.46$, $\theta = 1°$. The time is (*a*) 2.5 ± 0.3 non-dimensionally or 1.55 s on the videotape record; (*b*) 5.1 ± 0.3 non-dimensionally or 3.07 s on the videotape record; (*c*) 7.2 ± 0.3 non-dimensionally or 4.29 s on the videotape record. Image enhancement as figure 2.

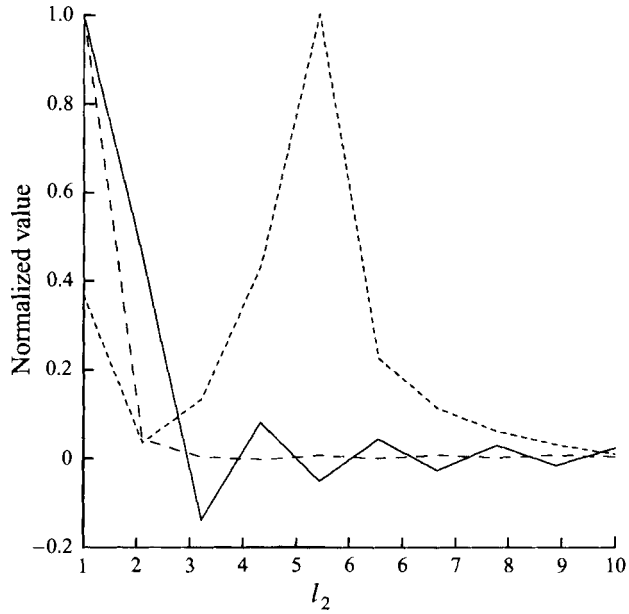

FIGURE 8. Relative interaction strengths of ten $(2, l_2, 0)$ modes with the (1,1,1) mode. The solid line is $c_{211\dagger} + c_{21\dagger 1}$ (secondary driven by primary) and the dashed line is $c_{112} + c_{112\dagger}$ (primary driven by secondary), where subscript 1 is for the primary, (1,1,1) mode and subscript 2 is for a secondary, $(2, l_2, 0)$ mode. The dotted line is the closeness-to-resonant-triad quotient, Δ. Each line is normalized to its maximum value: $(c_{211\dagger} + c_{21\dagger 1})$, 1.451; $(c_{112} + c_{112\dagger})$, 3.437; Δ, 2.324

to be present at this stage, apparently superimposed on the blobs and kinks that the dyelines also reveal. Indeed, it was noted in M92 that the visualizations at this stage using a reflective-flake technique show only evidence of the (1,1,1) mode. It was inferred by M94 that this was due to the relative weakness of the flow corresponding to the kink, and to its time dependence.

This behaviour confirms that the flow can be described by linear inviscid theory for only about 5 revolutions after the commencement of forcing. The hypothesis that the nonlinear interaction of the (2,1,0) mode with the (1,1,1) mode is occurring cannot be supported. The hypothesis was that a simple nonlinear interaction would explain the dyeline kink. The kink was a structure of smaller scale than the (1,1,1) mode but apparently consistent with a flow caused by the presence of a low-order mode like (2,1,0). The test shows that the departure from the linear inviscid description fundamentally involves small-scale motion of about a fifth of the tank radius. Moreover, the small-scale motion is not consistently small across the tank radius. This is consistent with the indications from §4 that complex nonlinear interactions are likely to prevail.

It is not likely that an interaction with a single, but higher-order, $(2, l_2, 0)$ mode is responsible for the small-scale behaviour. A higher-order $(2, l_2, 0)$ mode could not alone cause the large-scale kink in the tank centre, as well as the small-scale behaviour at half the tank radius. There is no particular reason for an interaction with a single high-order mode to be favoured over an interaction with a single low-order mode. To illustrate this, the interaction strengths of some $(2, l_2, 0)$ modes (the $c_{n\alpha\beta}$ defined in the Appendix) were calculated. These integrals were calculated numerically by a third-order NAG finite-difference routine. The closeness to resonance was also calculated. The result for interactions of ten $(2, l_2, 0)$ modes with the (1,1,1) mode is given in figure 8. The solid line is $c_{211\dagger} + c_{21\dagger 1}$, where subscript 1 is for the (1,1,1) mode and

subscript 2 is for a $(2, l_2, 0)$ mode. This indicates the extent to which a $(2, l_2, 0)$ mode is 'driven' by the (1,1,1) mode. The dashed line is $c_{112} + c_{112^*}$, indicating the extent to which the (1,1,1) mode is in turn 'driven' by a $(2, l_2, 0)$ mode. The dotted line is the closeness-to-resonant-triad quotient, Δ. Each line is normalized to its maximum value.

From figure 8, higher-order $(2, l_2, 0)$ modes interact with the (1,1,1) mode more weakly than the (2,1,0) mode. The interaction is closest to resonance at (2,5,0). However, this corresponds to $1/\Delta = 0.4305$, which is not particularly close to resonance. The closest triad computed in §4 – the tallest spike in figure 5(f) – corresponds to $1/\Delta = 0.00061$.

6. Discussion and conclusions

Contained inertia-wave systems are ones in which even the linear theory has peculiarities. Because of the ill-posed nature of the problem, organized stable solutions are not guaranteed for any geometry, and it appears that the appearance of wave modes is an unstable phenomenon.

Further confirmation has been found that the contained inertia-wave system is one in which linear inviscid theory, while accurately predicting the resonant frequencies of modes in certain special geometries (e.g. McEwan 1970; M92), rapidly breaks down. It is clear that the dyeline distortions (the kinks and outflows) described here and in M94 are not consistent with the forced response expected from linear inviscid theory. Nor are they consistent with the transient response (M94). Furthermore, the higher-order forced modes which contribute to the linear response must all have the same time dependence as the mode closest to resonance. Therefore they cannot account for distortions that rotate with the container.

The formation of small-scale structures has been detailed, notably the dyeline kinks and outflows. These consistently occur at the nodal planes of the (1,1,1) and (3,1,1) modes. The number of small-scale structures is therefore consistent with the axial wavenumber of these modes. The behaviour near the resonance of the (5,2,1) mode is more complex. However, instabilities again appear at nodal planes. The significance of the nodal planes is not yet clear. It should be noted that the distortions, initially at least, represent flows of a magnitude significantly lower than the primary forced response. In general, more catastrophic breakdowns of the flow (M92) will occur later in time than the present experiments could examine.

One possibility is that the dyeline distortions are of viscous origin. The coplanar outflows noted in §3.1 are more suggestive of dye spreading along weak internal shear layers (Wood 1966; Kerswell 1995) than of, say, weakly nonlinear interactions with other modes. In particular, the development of the bow-tie pattern shows an angularity more consistent with intersecting characteristics than with the recirculation zones of secondary modes.

Indications that the dyeline distortions are due to shear layers along characteristic surfaces would be: a coincidence in the angles of the distortions and the characteristic angle; a consistency in the velocity scales with those predicted theoretically for the shear layers; and a continuation of the oscillatory time dependence of the primary forced response. The distortions begin at the nodal planes; there is no particular reason why the characteristics should intersect at the nodal planes, but it may be that their angle simply defines the direction of propagation of an instability. For the (1,1,1)-mode experiments in M94, the characteristic angle is about 24° while the observed dyeline distortion is at about 70–80°; here there is no coincidence. For the

(3,1,1) mode experiments, the characteristic angle at $\omega = 1.22$ is 55°; the observations indicate a reasonable coincidence with this angle. For the (5,2,1) mode there is again no coincidence between the characteristic angle and the angle of the outflow to the vertical. Considering the scale of the flows, various magnitudes have been calculated for the shear layers. However, they may be assumed to have values between the Ekman layer at $E^{1/2}$ and the Stewartson layer at $E^{1/4}$ (Greenspan 1968). If the latter case were taken, the shear-layer scale for the (1,1,1)- and (3,1,1)-mode experiments could reach the same order of magnitude as the observed distortion flows. However, the shear layers are supposed to accompany the oscillatory forced response and indeed are driven by them, whereas the observations show the flow losing its oscillatory time dependence and linear mode structure.

The weakly nonlinear interactions in a cylindrical container are inherently ubiquitous. A test experiment illustrates that the most naïve interpretation of weakly nonlinear theory fails to explain the departure from linear inviscid theory. The complexity of potential weakly nonlinear interactions is a direct result of the transcendental nature of the dispersion relation for the cylindrical modes. Similar complexity might be expected in spheroidal containers. It would be particularly interesting to experimentally investigate inertial oscillations in a rectilinear container, to see if the breakdown phenomena are equally prevalent. If they are, then more fundamental phenomena such as elliptical-flow instabilities are liable to be the root cause or causes of the breakdowns; this will be discussed shortly.

It was noted in §1 that experimental evidence associating a mean circulation with breakdowns of inertia-wave modes does exist. However, the precise nature of the association between a mean circulation and the various breakdown phenomena has not yet been elucidated. Mean circulations are not evident in the experiments reported here or in M94. The small mean circulation expected (Thompson 1970) on the basis of asymptotic theory is too small to be observed in the present experiments. Nor could it significantly influence the tuning of the system near resonance, via the mechanism derived by Gunn & Aldridge (1990). Nevertheless, a mean circulation may be important in later stages of the breakdown, particularly the more dramatic 'violent-collapses' (M92), if the mean circulation is in fact a flow with elliptical streamlines.

An elliptical flow effectively forms one member of a nonlinear triad with a cylindrical inertia-wave mode (Waleffe 1990). Studies of elliptical-flow instabilities such as that of Waleffe (1990) begin with a basic flow that has elliptical streamlines, which through the nonlinear mechanism creates an unstably-growing cylindrical inertia-wave mode. The present experiments, and similar studies already detailed in §1, begin with a basic flow that is a cylindrical inertia wave mode. Perhaps the same mechanism is at work, in this case generating an elliptical flow as part of the breakdown process.

Whether or not the dyeline distortions reported here and in M94 are part of the same process in unclear. However, it is likely that they, along with a great number of approximate-resonant-triad interactions, are separate phenomena exhibited by the extraordinarily rich contained inertia-wave system.

The bulk of this work was done while I was a PhD student in the Department of Applied Mathematics and Theoretical Physics, University of Cambridge. I should like to thank my supervisor, Dr Paul Linden, as well as my colleagues, in particular Dr David Tan, Prof Michael McIntyre and Dr John Jackson, for many helpful discussions. This work was done as part of a project funded by the British National Space Centre / Royal Aerospace Establishment and managed by British Aerospace

PLC. Advice from anonymous reviewers was appreciated. Some of the final numerical calculations were done at the School of Mathematics of the University of New South Wales.

Appendix. Derivation of the interaction equations

Firstly, refer to the original, fully nonlinear momentum equation (2.1). Now the dynamic terms are no longer assumed to be small, and therefore no expansion of $\boldsymbol{u}$ and p in powers of the small parameter θ is made. Note, however, that terms containing θ will still appear. These are present because the kinematic forcing term, which arises from the variation of the axis of spin owing to the forced precession, was originally simplified under the assumption that θ is small, i.e. the time-variant vector $\hat{\boldsymbol{K}}$ was expanded to $O(\theta)$. This has the effect of simplifying the forcing term in the equation but does not affect the nonlinear terms. The inviscid approximation is maintained. The momentum equation is now given by

$$\frac{\partial \boldsymbol{u}}{\partial t} + (\boldsymbol{u}\cdot\nabla)\boldsymbol{u} + \omega\hat{\boldsymbol{k}}\times\boldsymbol{u} + \theta(\omega-2)(r\cos(\phi+t))\hat{\boldsymbol{k}} - \theta(\omega-2)\begin{pmatrix} w\sin t \\ w\cos t \\ -v\cos t - u\sin t \end{pmatrix} = -\nabla p. \tag{A 1}$$

The inhomogeneous term, $\theta(\omega-2)(r\cos(\phi+t))\hat{\boldsymbol{k}}$, comes from the time-dependent 'cross-Coriolis' term and the time-dependent $O(\theta)$ part of the centrifugal term that cannot be expressed as ∇p, both of which are due to the forced precession.

The real velocity and pressure are expressed as a sum of the complex spatial eigenmode functions $\boldsymbol{U}_n$ and Q_n, multiplied by arbitrary complex time-varying amplitudes A_n,

$$\boldsymbol{u} = \sum_{n=1}^{\infty}(A_n\boldsymbol{U}_n), \tag{A 2}$$

and

$$p = \sum_{n=1}^{\infty}(A_nQ_n), \tag{A 3}$$

where the Q_n are given by (2.6) and the $\boldsymbol{U}_n = (U_n, V_n, W_n)$ are given (M94) by

$$U_n = \mathrm{i}\frac{1}{1-\omega_n{}^2}\left[\frac{\mathrm{d}J_m(2\lambda_nr)}{\mathrm{d}r} + m\omega_n\frac{1}{r}J_m(2\lambda_nr)\right]\cos\left[k\pi(z/h+\tfrac{1}{2})\right]\,\mathrm{e}^{\mathrm{i}m\phi}, \tag{A 4}$$

$$V_n = \frac{-1}{1-\omega_n{}^2}\left[\omega_n\frac{\mathrm{d}J_m(2\lambda_nr)}{\mathrm{d}r} + m\frac{1}{r}J_m(2\lambda_nr)\right]\cos\left[k\pi(z/h+\tfrac{1}{2})\right]\,\mathrm{e}^{\mathrm{i}m\phi}, \tag{A 5}$$

$$W_n = -\mathrm{i}\frac{k\pi}{h}J_m(2\lambda_nr)\sin\left[k\pi(z/h+\tfrac{1}{2})\right]\,\mathrm{e}^{\mathrm{i}m\phi}. \tag{A 6}$$

To each index n there corresponds one combination of the wavenumber indices k, l and m for a mode.

The notation $\omega < 0$ will be used to denote modes which represent waves travelling with a phase velocity in the opposite sense to $\omega > 0$ modes. As noted in M94, because of the nature of the dispersion relation, waves with the same k, l and m but opposite direction of phase propagation have a different spatial structure. They are distinctly different modes, and, reflecting this, the argument of the Bessel functions λ is different.

In the experiments of M92 and M94, only modes with positive ω could be directly forced by the apparatus; however, in considering the nonlinear interactions, all modes will have to be reckoned with. The conjugation operation will be denoted by the † superscript.

Because the wavenumbers in the radial direction need not sum to permit nonlinear interaction, the interaction equations cannot be written down by simply equating those terms that satisfy a resonant triad condition. Accordingly, the orthogonality properties of inertia-wave modes must be used. Any such modes can be shown to be orthogonal (Greenspan 1968). Inserting (A 2) and (A 3) into (A 1), multiplying by the conjugate of the nth spatial eigenfunction and integrating over the container volume gives

$$\frac{\partial A_n}{\partial t} = \mathrm{i}\frac{\omega}{\omega_n}A_n + \mathrm{i}\sum_{\alpha=1}^{\infty}\sum_{\beta=1}^{\infty}\left(c_{n\alpha\beta}A_\alpha A_\beta + c_{n\alpha\beta^\dagger}A_\alpha A_\beta^\dagger\right) + \theta(1-\tfrac{1}{2}\omega)\textstyle\sum_{\alpha=1}^{\infty} d_{n\alpha}A_\alpha + \theta f_n\,\mathrm{e}^{\mathrm{i}t}, \tag{A 7}$$

where the $c_{n\alpha\beta}$, $c_{n\alpha\beta^\dagger}$ and the f_n are real and the $d_{n\alpha}$ are complex. Here

$$\frac{\mathrm{i}}{\omega_n} = -\frac{\langle\hat{\boldsymbol{k}}\times\boldsymbol{U}_\alpha\rangle}{\langle\boldsymbol{U}_n\rangle}, \tag{A 8}$$

$$\mathrm{i}c_{n\alpha\beta} = -\frac{\langle(\boldsymbol{U}_\alpha\cdot\nabla)\boldsymbol{U}_\beta\rangle}{\langle\boldsymbol{U}_n\rangle}, \tag{A 9}$$

$$d_{n\alpha} = -2\frac{1}{\langle\boldsymbol{U}_n\rangle}\int_{\mathscr{V}}\begin{pmatrix} W_\alpha\sin t \\ W_\alpha\cos t \\ -V_\alpha\cos t - U_\alpha\sin t\end{pmatrix}\cdot\boldsymbol{U}_n^\dagger\,\mathrm{d}\mathscr{V}, \tag{A 10}$$

and

$$f_n = \frac{\mathrm{i}4\pi(2-\omega)}{\langle\boldsymbol{U}_n\rangle}\int_0^{1/2} r^2J_1(2\lambda_n r)\,\mathrm{d}r, \quad m=1 \text{ and } k \text{ odd}, \qquad = 0, \quad m\neq 1 \text{ or } k \text{ even}, \tag{A 11}$$

where the inner-product integral is defined as

$$\langle\boldsymbol{X}\rangle = \int_{\mathscr{V}}\boldsymbol{X}\cdot\boldsymbol{U}_n^\dagger\,\mathrm{d}\mathscr{V}, \tag{A 12}$$

for any complex vector function $\boldsymbol{X}$, with $\mathrm{d}\mathscr{V} = r\,\mathrm{d}r\,\mathrm{d}\phi\,\mathrm{d}z$. Steps in the derivation from the momentum equation of the linear version of (A 7) are given in M94.

Because the inhomogeneous (or forcing) term is even in z, its inner-product integral, and hence f_n, is zero unless k_n is odd, which is when the $\hat{\boldsymbol{k}}$-component of velocity is an even function in z. Similarly, f_n is zero unless the forcing term is projecting onto a mode that matches its unity azimuthal wavenumber, $m = 1$.

Considering the nonlinear terms, their inner-product integrals in the axial and azimuthal directions collapse on to sums of delta functions expressing the conditions

$$\{k_n, k_\alpha, k_\beta : \pm k_n = \pm k_\alpha \pm k_\beta\} \cup \{m_n, m_\alpha, m_\beta : \pm m_n = \pm m_\alpha \pm m_\beta\}. \tag{A 13}$$

However, the radial integrals do not show this behaviour. They would not be expected to unless the arguments λ_n of the Bessel functions were large, justifying an asymptotic representation of the Bessel functions as approximately sinusoidal. Combinations of axial and azimuthal wavenumbers satisfying the condition (A 13) will be called

interacting combinations. Sets of modes with interacting combinations of wavenumbers will be called *interacting sets.* An *expressed* mode has non-zero f_n and hence can be precessionally forced. The *primary* mode is the expressed mode in a forced system with resonant frequency ω_n closest to the excitation frequency ω.

If, in addition to the condition (A 13) on the axial and azimuthal wavenumbers, the temporal frequencies of three modes are such that the condition

$$\left\{\frac{1}{\omega_n}, \frac{1}{\omega_\alpha}, \frac{1}{\omega_\beta} : \pm\frac{1}{\omega_n} = \pm\frac{1}{\omega_\alpha} \pm \frac{1}{\omega_\beta}\right\} \tag{A 14}$$

is satisfied, the interacting set is called a *resonant triad.* In this case energy can easily be transferred from a primary mode to two secondary modes or 'parasites', which could be non-expressed ($f_n = 0$); they are brought into existence solely by nonlinear interaction. However, in this system, (A 14) cannot be exactly satisfied and thus there are no exact resonant triads. This, along with the lack of a condition on the radial wavenumber, is a feature of the dispersion relation. For the cylindrical modes, the dispersion relation is governed by a transcendental equation (from (2.7) and (2.8)), with roots that are densely, rather than discretely spaced.

Note that as the $d_{n\alpha}$ are functions of time, the interaction equations would be non-autonomous if θ were not small.

The radial integrals of the nonlinear term, $\int_0^{1/2} ((\boldsymbol{U}_\alpha \cdot \nabla)\boldsymbol{U}_\beta) \cdot \boldsymbol{U}_n^\dagger r \, \mathrm{d}r$, are particularly hard to evaluate; recurrence relations for the Bessel functions that would enable an elegant evaluation of all these integrals cannot be found. Most of them, of course, may be ignored since they correspond to non-interacting combinations of the axial and azimuthal wavenumbers.

REFERENCES

ALDRIDGE, K. D. & LUMB, L. I. 1987 Inertial waves identified in the Earth's fluid outer core. *Nature* **325**, 421–423.

ALDRIDGE, K. D. & STERGIOPOULOS, S. 1991 A technique for direct measurement of time-dependent complex eigenfrequencies of waves in fluids. *Phys. Fluids* A **3**, 316–327.

BEARDSLEY, R. C. 1970 An experimental study of inertial waves in a closed cone. *Stud. Appl. Maths* **49**, 187–196.

CRAIK, A. D. D. 1985 *Wave Interactions and Fluid Flows.* Cambridge University Press.

FULTZ, D. 1959 A note on overstability, and the elastoid-inertia oscillations of Kelvin, Solberg and Bjerknes. *J. Met.* **16**, 199–208.

GANS, R. F. 1984 Dynamics of a near-resonant fluid-filled gyroscope. *Am. Inst. Aeronaut. Astronaut. J.* **22**, 1465–1471.

GLEDZER, E. B., DOLZHANSKII, F. V. & OBUKHOV, A. M. 1989 Instability of elliptical rotation and simple models of vortex fluid flows. *Abstracts, Euromech 245: The effect of background rotation on fluid motions, Dept. Applied Maths & Theor. Physics, Cambridge, UK, April 10–13, 1989.*

GLEDZER, E. B. & PONOMAREV, V. M. 1992 Instability of bounded flows with elliptical streamlines. *J. Fluid Mech.* **240**, 1–30.

GREENSPAN, H. P. 1968 *The Theory of Rotating Fluids.* Cambridge University Press.

GUNN, J. S. & ALDRIDGE, K. D. Inertial wave eigenfrequencies for a non-uniformly rotating fluid. *Phys. Fluids* A **2**, 2055–2060.

HENDERSON, G. A. & ALDRIDGE, K. D. 1992 A finite-element method for inertial waves in a frustrum. *J. Fluid Mech.* **234**, 317–327.

JOHNSON, L. E. 1967 The precessing cylinder. *Notes on the 1967 Summer Study Program in Geophysical Fluid Dynamics at the Woods Hole Oceanographic Institution.* Ref No. 67–54, pp. 85–108.

KELVIN, LORD 1880 Vibrations of a columnar vortex. *Phil. Mag.* **10**, 155–168.

KERSWELL, R. R. 1993 The instability of precessing flow. *Geophys. Astrophys. Fluid Dyn.* **71**, 107–144.

KERSWELL, R. R. 1995 On the internal shear layers spawned by the critical regions in oscillatory Ekman boundary layers. *J. Fluid Mech.* **298**, 311–325.

KOBINE, J. J. 1995 The dynamics of inertia waves in a rotating and precessing cylinder. *J. Fluid Mech.* **303**, 233–252.

MALKUS, W. V. R. 1968 Precession of the Earth as the cause of geomagnetism. *Science* **160**, 259–264.

MALKUS, W. V. R. 1989 An experimental study of the global instabilities due to the tidal (elliptical) distortion of a rotating elastic cylinder. *Geophys. Astrophys Fluid Dyn.* **48**, 123–134.

MALKUS, W. V. R. & WALEFFE, F. A. 1991 Transition from order to disorder in elliptical flow: a direct path to shear flow turbulence. *Advances in Turbulence 3* (ed. A. V. Johansson & P. H. Alfredsson), pp. 197–203.

MANASSEH, R. 1991 Inertia wave breakdown: experiments in a precessing cylinder. PhD thesis, University of Cambridge.

MANASSEH, R. 1992 Breakdown regimes of inertia waves in a precessing cylinder. *J. Fluid Mech.* **243**, 261–296 (referred to herein as M92).

MANASSEH, R. 1993 Visualization of the flows in precessing tanks with internal baffles. *Am. Inst. Aeronaut. Astronaut. J.* **31**, 312–318.

MANASSEH, R. 1994 Distortions of inertia waves in a rotating fluid cylinder forced near its fundamental mode resonance *J. Fluid Mech.* **265**, 345–370 (referred to herein as M94).

MCEWAN, A. D. 1970 Inertial oscillations in a rotating fluid cylinder. *J. Fluid Mech.* **40**, 603–640.

MCEWAN, A. D. 1971 Degeneration of resonantly-excited standing internal gravity waves. *J. Fluid Mech.* **50**, 431–448.

MCEWAN, A. D. 1983 Internal mixing in stratified fluids. *J. Fluid Mech.* **128**, 59–80.

MCEWAN, A. D., MANDER, D. W. & SMITH, R. K. 1972 Forced resonant second-order interaction between damped internal waves. *J. Fluid Mech.* **55**, 589–608.

MCINTYRE, M. E. & NORTON, W. A. 1990 Dissipative wave-mean interactions and the transport of vorticity or potential vorticity *J. Fluid Mech.* **212**, 403–435.

POINCARÉ, H. 1910 Sur la precession des corps deformables. *Bull. Astronomique* **27**, 321–56.

SCOTT, W. E. 1975 The large amplitude motion of a liquid-filled gyroscope and the non-interaction of inertial and Rossby waves. *J. Fluid Mech.* **72**, 649–660.

STERGIOPOULOS, S. & ALDRIDGE, K. D. 1982 Inertial waves in a fluid partially filling a cylindrical cavity during spin-up from rest. *Geophys. Astrophys. Fluid Dyn.* **21**, 89–112.

THOMPSON, R. 1970 Diurnal tides and shear instabilities in a rotating cylinder. *J. Fluid Mech.* **40**, 737–751.

THORPE, S. A. 1966 On wave interactions in a stratified fluid. *J. Fluid Mech* **24**, 737–751.

WALEFFE, F. 1990 On the three dimensional instability of strained vortices. *Phys. Fluids* A **2**, 76–80.

WHITING, R. D. 1981 An experimental study of forced asymmetric oscillations in a rotating liquid filled cylinder. *United States Army Armament Command Ballistic Research Labs. Rep.* ARBRL-TR-02376.

WOOD, W. W. 1966 An oscillatory disturbance of rigidly rotating fluid. *Proc. R. Soc. Lond.* A **293**, 181–212.